KM-SCALE SHORELINE SAND WAVES: NUMERICAL MODELLING AND OBSERVATIONS

Jaime Arriaga[1], Francesca Ribas[2], Ismael Mariño[3], Albert Falqués[4]

Km-scale shoreline sand waves have been studied with a quasi two dimensional model (Q2D-morfo model) and with observations from a populated coastal zone in Yucatán (México) with frequent human interventions. The model was modified to improve the physics in the case of large amplitude shoreline sand waves that develop due to the high angle wave instability (HAWI). The modified version of the model can better reproduce the formation of large-amplitude shoreline sand waves, compared with the original model. Shorelines of Yucatán, from 2004 to 2012, were digitized and analyzed. Although undulations can be observed, they do not exhibit clear migration or growth, an indication of being in the limit of instability, in accordance with the results of the model.

Keywords: Shoreline sand waves; High angle wave instability; Yucatán coast

INTRODUCTION

Wavy morphological features can be seen in different parts of the coastal area: below the sea surface (ripples, crescentic sand bars), in the dry beach (dunes) and in the swash zone (cusps). During the 80's and the 90's, it was believed that they have been caused by a certain template hydrodynamic forcing, but more recently they were successfully explained by a self organized behavior of the morphodynamic system (Coco and Murray, 2007).

In the present study we focus on rhythmic morphological patterns with a larger spatial scale, in the range of 1-10 km, called shoreline sand waves, which are undulations of the shoreline that extend as bathymetric perturbations across the surf and shoaling zones. We name them km-scale shoreline sand waves (KSSW) to make a distinction with larger scale shoreline features (e.g., cuspate coasts). There are documented observations of KSSW from the 50's (Bruun, 1954) until now (Kaergaard et al., 2012; Idier and Falqués, 2014).

Ashton et al. (2001) presented a potential mechanism that could explain the existence of shoreline undulations: the so-called high angle wave instability (HAWI). When waves with a very oblique angle of incidence (above 42°) are persistent, a distortion in the littoral drift occurs giving rise to undulations in the shoreline. Their approach is based on the one line model philosophy (Pelnard-Considère, 1956), where the changes in the shoreline are governed by the gradients in the alongshore sediment transport rate driven by oblique breaking waves, Q (Komar, 1998), and the shape of the profile shifts with the shoreline position. The computation of Q is typically made with the CERC formula, and it is function of the wave height H_b and angle α_b (relative to the shoreline) at the breaking point. The feedback between the bathymetry and the wave field is an essential mechanism behind HAWI and it is the critical difference with the traditional one line models (which assume that H_b and α_b are unaffected by the shoreline changes). In fact, as Ashton et al. (2001) pointed out, a shoreline undulation (with the corresponding bathymetric undulation) leads to alongshore gradients in both α_b (due to refraction) and H_b (due to wave energy spreading). For low wave angles, α_b perturbations are dominant with a stabilizing effect leading to the diffusion of undulations. For high angle waves, H_b perturbations are dominant and lead to growth and migration of the undulations. However, important simplifications were made by Ashton et al. (2001): i) the shoreline perturbations extended offshore up to the wave base without decaying; ii) the shifts of the cross-shore profiles were instantaneous; iii) wave transformation was calculated over rectilinear depth contours that were parallel to the evolving shoreline. This assumptions are only suitable for very large scale features.

Other approaches have been explored. Falqués and Calvete (2005) made a linear stability analysis that provided more understanding of the dynamics of the sand waves. Their model could describe bathymetric perturbations that decayed at a finite offshore distance and curvilinear depth contours. They found that a higher angle was needed for the undulations to grow and also that a dominant wavelength arose, contrary to the continuously increasing wavelength predicted by Ashton et al. (2001). They also made important simplifications: i) the offshore decay distance of the bathymetric perturbations was fixed; ii) the shifts of the cross-shore profiles were still instantaneous. Besides, the linear stability analysis implies perturbations with infinitesimal amplitude, ignoring non linear effects.

[1]Department of Applied Physics, Universitat Politècnica de Catalunya, Barcelona, Spain
[2]Department of Applied Physics, Universitat Politècnica de Catalunya, Barcelona, Spain
[3]Coastal Processes and Physical Oceanography Laboratory, CINVESTAV-IPN, México
[4]Department of Applied Physics, Universitat Politècnica de Catalunya, Barcelona, Spain

van den Berg et al. (2012) presented a quasi 2D numerical model where the offshore perturbation extent was dynamic and the shifts of the cross-shore profiles were no longer instantaneous. They found that the minimum wave incidence angle required for the instability was 45° at the depth of closure, an angle much greater than the one found by Ashton et al. (2001), which was of 42° at the base of the shoreface. The growth rate was favored by high amplitude waves of short periods. Finally, an analysis confirmed that wave energy spreading due to refraction over the curvilinear bathymetric perturbations is essential for HAWI and that wave focusing explains the emergence of an optimal wavelength of the undulations. However, the numerical implementation of the model of van den Berg et al. (2012) was such that the slope of the undulation (relation between amplitude and wavelength of the sand waves) could not exceed ~ 13° and assumed the cross-shore sediment transport to have always only one component (perpendicular to the initial shoreline).

The aim of the present contribution is to gain understanding on the non linear evolution of shoreline sand waves of significant amplitude. For this, several improvements have been introduced in the model of van den Berg et al. (2012). Firstly, we have modified the numerical implementation by no longer treating the shoreline as a boundary condition. With this change the first limitation of van den Berg (2012) is overcome. Secondly, we have changed the direction of the cross-shore transport so that it is points into the direction of maximum change of the bathymetric lines, i.e. the local cross-shore direction felt by the waves. This is more realistic in case of large-amplitude shoreline sand waves. The other improvements will be described in section 2. The results of the modified model are compared with those of the old version in order to check the effect of these improvements (section 3). In addition, in order to compare model results with data, we have analyzed the Yucatán coast, extracting shorelines of different years, from 2003 to 2013 (section 4). This coast has a dominant transport direction from east to west with waves of large angle of incidence, and small height and period, which suggest that HAWI could be acting. We end up applying the model to the Yucatán coast and comparing the numerical results with the field data (section 5).

NUMERICAL MODEL

The Q2D-morfo model is a simplified version of the 2DH models. The model computes the sediment transport from the wave field without determining the mean hydrodynamics. Consequently, the dynamics of small scale surfzone features, like rip currents, can not be reproduced but this simplification, besides making feasible to perform large scale simulations, is also reasonable. A cartesian frame with horizontal coordinates x, y and upward vertical coordinate z is used, where y runs along the initial mean shoreline orientation. The modeled area is a rectangular domain, $0 < x < L_x, 0 < y < L_y$. The unknowns are the moving shoreline $x = x_s(y, t)$, and the changing bed level, $z = z_b(x, y, t)$. The domain is discretized in cells Δx of cross-shore and Δy of alongshore.

Typically, in morphodynamic numerical models the domain is divided between dry cells and wet cells and the equations are only solved in the wet domain. Nevertheless this approach has proven difficult in its implementation because the shoreline, which is highly dynamic, has to be treated as a boundary condition (van den Berg et al., 2012). We no longer make a distinction in the nature of the cells in the improved version of the model and the shoreline is considered as fuzzy, i.e. as a transition area between the dry and wet beach. This implies that the equations are solved in all the domain and that all the functions have to be defined also in the dry zone.

Sediment Transport

The bed level evolution is described by the sediment mass conservation equation,

$$\frac{\partial z_b}{\partial t} + \frac{\partial q_x}{\partial x} + \frac{\partial q_y}{\partial y} = 0 \ , \tag{1}$$

where $\vec{q} = (q_x, q_y)$ is the depth integrated sediment flux and the bed porosity factor is included for convenience in $\vec{q}$.

The sediment flux is decomposed as

$$\vec{q} = \vec{q_C} + \vec{q_E} \ . \tag{2}$$

The first term represents the littoral drift caused by the breaking waves and the second term represents a diffusive transport that makes the bathymetry relax to an equilibrium one.

The transport rate Q, corresponding to the total littoral drift, is computed with the CERC formula (Komar, 1998),

$$Q = \mu H_b^{5/2} sin(2\alpha_b) \ , \tag{3}$$

where $H_b(y)$ is the root mean square wave height at breaking, $\alpha_b(y) = \theta_b(y) - \phi_s(y)$ is the angle between the wave fronts at breaking $\theta_b(y)$ and the coastline $\phi_s(y)$, and the constant μ controls the magnitude of the transport with the default value being $\mu = 0.2\mathrm{m}^{1/2}\mathrm{s}^{-1}$ (which roughly corresponds to a value of the CERC constant of $K_1 = 0.7$). Q is the total sediment transport rate along a cross-shore profile due to breaking waves. For rectilinear coasts, the profile is perpendicular to the rectilinear coast and there is one value of Q for each y-profile ($Q(y)$). Nevertheless, when a coast has pronounced undulations, this treatment is not correct. To illustrate this, imagine a swimmer who wants to arrive to the coast which is undulating. He must head to the closest point (not necessarily of the same y-profile) and, similarly, the current he feels corresponds to the waves that are breaking at the closest point. So, in the improved version of the model, Q is computed for each cell $Q(x, y)$ instead of for each profile. This implies that the value of H_b and θ_b used for each cell is the one corresponding to the point of the breaking line that is closest to the coordinates (x, y) of the cell and the value for ϕ_s is the one corresponding to the closest point of the shoreline (only when the shoreline is rectilinear, these points lay on the same cross-shore profile as (x, y)).

The corresponding sediment flux term, $\vec{q}_C$ in equation (2), is computed by multiplying the transport rate Q by a shape function $f(x_c)$, where x_c is the distance to the closest shoreline point including the swash zone. The shape of f is related to the longshore current profile (Komar, 1998). In the modified version of the model, $\vec{q}_C$ points into the direction of the bathymetric lines, $\phi_{bat}(x, y)$,

$$\vec{q}_c = f(x_c)Q(x, y)\,(\sin(\phi_{bat}(x, y)), \cos(\phi_{bat}(x, y))) \ , \tag{4}$$

with

$$f(x_c) = \frac{4}{\sqrt{\pi}L^3} x_c^2 e^{-(x_c/L)^2} \ . \tag{5}$$

Here, $L = 0.8X_b + x_p$, X_b is the distance between the closest breaking point x_b and the closest local shoreline point x_s, therefore representing the surfzone width and x_p elongates the function to take into account the transport in the swash zone. The breaking point $x_b(y)$ is defined as the most offshore point where $H(x, y) \geq \gamma_b D(x, y)$, where D is the water depth and γ_b is the breaking coefficient. $x_s(y)$ is computed with an interpolation between the last dry cell and the first wet cell.

The orientation of the coast, $\phi_s(y)$, needed to calculate Q, is computed as an averaged orientation of the bathymetric contours in the surfzone with respect to the y-axis rather than the coastline orientation itself. This seems appropriate because this is the orientation that actually affects the waves at breaking.

$$\sin\phi_s(y) = \overline{\frac{\partial z_b}{\partial y}} \Big/ \sqrt{\left(\overline{\frac{\partial z_b}{\partial x}}\right)^2 + \left(\overline{\frac{\partial z_b}{\partial y}}\right)^2} \ , \tag{6}$$

where the average is computed within a rectangular box with a cross-shore length L_{box}, an alongshore length $2 * L_{box}$, where $L_{box} = B * X_b$ and the default value of the constant B is 2. In a similar way, the orientation of the bathymetric lines, $\phi_{bat}(x, y)$ in equation (4), is computed as an average within a rectangular box with default values of 30 m in its cross-shore side and 100 m in its alongshore side.

The second term in equation (2), the diffusive transport $\vec{q}_E$ that drives the bathymetry to an equilibrium, is computed as

$$\vec{q}_E = -\gamma\left(\vec{\nabla} z_b + \beta_E(\cos\phi_{bat}, -\sin\phi_{bat})\right) \ , \tag{7}$$

where γ is a diffusive coefficient and its physical basis is the diffusivity caused by breaking waves (see the details of its computation in van den Berg et al. (2012)) and β_E is the slope of the equilibrium bathymetry. The equilibrium bathymetry is assumed to be alongshore uniform and its cross-shore profile corresponds to a modified Dean profile for the wet beach. For the swash zone and dry beach, the profile is assumed to

follow an exponential function which tends to the height of the dune across a distance related to the width of the swash zone. The local value of β_E for each cell is computed from this profile using the local depth.

At the offshore boundary, $x = L_x$, the bathymetry is assumed to relax to the equilibrium bathymetry within a certain decay distance λ_x. At the lateral boundary, van den Berg et al. (2012) assumed no diffusive transport and the sand waves made a swaying movement when crossing the boundary. In the improved version of the model, we have included the diffusive transport also at the lateral boundary, assuming a relaxation of the bathymetry to the equilibrium profile within an alongshore distance related to the wavelength of the sand waves. With this, the swaying movement diminishes significantly. For the computation of ϕ_s and ϕ_{bat} in the cells where the boxes cover an area beyond the domain an exponential decay to zero of the quantities is assumed within the same alongshore distance.

Waves

The wave field is computed in the domain from the offshore boundary to the breaking line having as input the wave height, period and angle given at the offshore boundary. We use the dispersion relation,

$$\omega^2 = gk\tanh(kD) \ , \tag{8}$$

the equation for wave number irrotationality,

$$\frac{\partial(k\sin\theta)}{\partial x} = \frac{\partial(-k\cos\theta)}{\partial y}, \tag{9}$$

and the wave energy conservation equation up to breaking,

$$\frac{\partial}{\partial x}\left(-c_g H^2\cos\theta\right) + \frac{\partial}{\partial y}\left(c_g H^2\sin\theta\right) = 0 \ . \tag{10}$$

Here, $\omega = 2\pi/T_p$ is the radian frequency, T_p is the peak period, $\vec{k} = k\,(-\cos\theta, \sin\theta)$ is the wave number vector, c_g is the group celerity and θ is the angle of the wave crest with respect to the y-axis. Wave diffraction and dissipation are not taken into account. Due to the slow change of the bathymetry, it is not necessary to compute the wave field at each time step and we compute it twice every day (in this contribution we use constant wave conditions).

COMPARISON BETWEEN MODELS

Setup of the default experiment

A default experiment is defined in order to compare the results between the original version of the model (van den Berg et al., 2012) and the modified version described in the previous section. The parameter setting can be seen in Table 1. The size of the simulation domain is $L_x = 1.5$ km by $L_y = 32.5$ km with 700 m of dry beach. The following modified Dean profile is considered,

$$Z(x) = -A\left((x+d)^{2/3} - d^{2/3}\right) \ , \tag{11}$$

Table 1: Default parameter setting of this study.

Symbol	Paramater	Default value
H_s	Offshore significant wave height	1.4 m
T_p	Offshore peak wave period	6 s
θ_o	Offshore wave angle	60^o
γ_b	Breaking ratio coefficient	0.5
ϵ	Diffusivity coefficient	0.05
Δx	Cross-shore grid size	6 m
Δy	Alongshore grid size	50 m
Δt	Time step	0.001 days
D_c	Depth of closure	7 m

where d introduces a small shift to avoid an infinite slope at the shoreline. The constants d and A are computed with the swash slope at the shoreline ($\beta = 0.03$) and a reference water depth $D_{ref} = 10$ m at the offshore position $x_{ref} = 700$ m. For the initial bathymetry, a shoreline perturbation with a Gaussian shape with a cross-shore width of 25 m and an alongshore width of 2 km is located at $y = 3$ km. This initial bump can be interpreted as a beach nourishment.

In order to describe and quantify the shape and dynamics of the sand waves, their amplitude and wavelength must be defined. The amplitude is defined as the distance between the cross-shore positions of the crest and its subsequent trough and the wavelength is twice the alongshore distance between these two points. An ideal sand wave, with these two quantities, is plotted in figure 2.

Shoreline evolution

The initial bump clearly triggers the formation of a sand wave train in both models (Figure 1 and 3) for the default parameter setting (Table 1). The initial bump grows in amplitude very slowly and migrates down drift. The first sand wave evolves quite similarly in both models, but the following sand waves appear in similar alongshore positions but differ greatly in amplitude (Figure 1). This already indicates that they have similar migration celerities and wavelengths but different growth rates. .

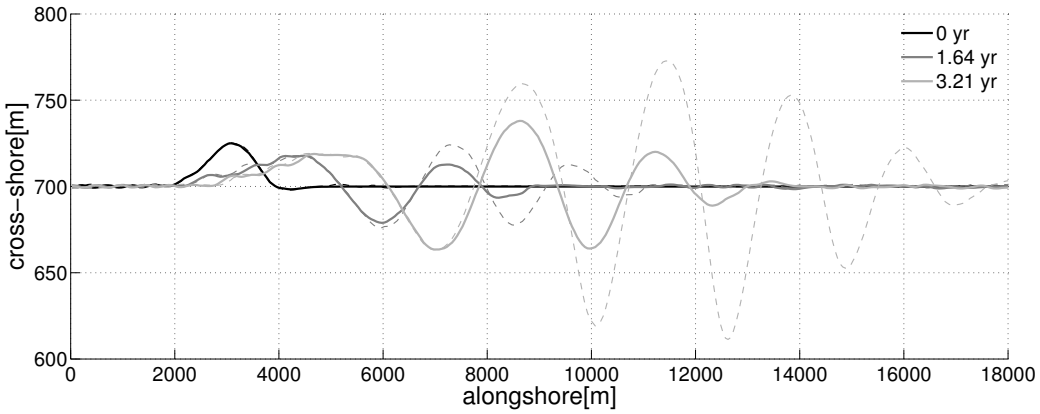

Figure 1: Shoreline evolution from 0 years to 3.21 years. Dashed lines correspond to the shoreline obtained with the original model. Continuous lines correspond to the ones obtained with the modified model.

Compared with the original model, the modified model can reproduce the evolution of the sand waves during a longer time period and the modeled sand waves reach a larger amplitude (Figure 3). The original model reproduces the evolution of the shoreline during 5.3 yr, when a numerical instability appears. However, after 4.2 yr an abrupt change can be observed in the third and fourth sand waves (Figure 3a). This occurs because at the flank of these two sand waves an angle of $\sim 13°$ is reached, which is a known numerical limitation of the original model (van den Berg et al., 2012). Thereby, we conclude that for this setup the prediction made by the original model is only reliable during 4.2 yr, reaching a maximum sand wave amplitude of 348 m. The modified model runs during 12.1 years, but we consider that the simulation is reliable only during the first 8.5 yr. In that moment, an abrupt change in the amplitude evolution of the third sand wave appears. This may be because the sand wave is in the limit of becoming a spit and, since the model can not handle this type of transformation, the unrealistic oscillations in the amplitude appear. The maximum sand wave amplitude at 8.5 yr is 760 m (Figure 3b) and the maximum angle in the flanks is 30°. In the modified model, the fifth to eight sand waves show a saturation of the amplitude growth but this result must be taken with care because it occurs for t>8.5 yr (the reliable simulation time, Figure 3).

We now compare the elapsing time between the moment when a sand wave appears and the moment when the following sand wave of the train appears. The appearance of a sand wave is defined as the moment when the undulation achieves an amplitude of 10 m. The elapsing time is 8 months (on average) in the original version of the model and 15 months in the modified version (Figure 3).

A Fourier analysis of the signal has been performed at different moments of the simulation (Figure 4). At the beginning there are no dominant wavelengths but as time passes a clear peak in the Fourier transform is observed. For the original model the peak is around $\lambda = 2600$ m whilst for the modified version it appears

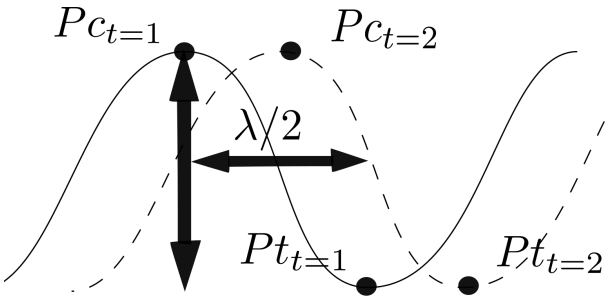

Figure 2: Definition sketch of a shoreline sand wave. *Pc* **is the position of the crest,** *Pt* **is the position of the trough.**

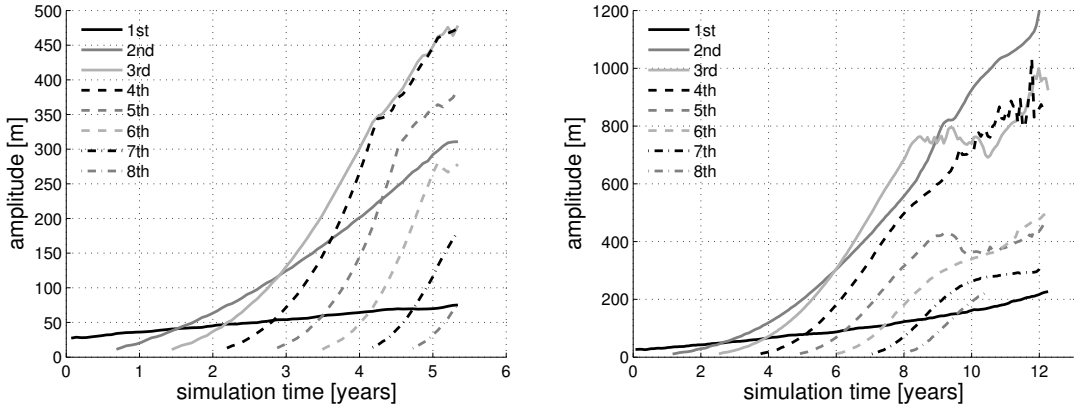

(a) original version **(b)** modified version

Figure 3: Time evolution of the amplitude of the individual sand waves of the sand wave train for the two versions of the model .

for a wavelength λ = 3200 m. In general, longer wavelengths are developed in the modified model. Figure 5 shown the time evolution of the wavelength of each sand wave. In the original model, for the 3 first sand waves the wavelength has a linear growth whilst the subsequent sand waves, which are hardly influenced by the initial perturbation, present a wavelength constant in time of about 2 km. In the modified model, the last sand waves show a wavelength around 2.2 km.

The asymmetry of the largest sand wave has also been quantified as the ratio between the slope down-drift of the crest and the slope up-drift of the crest of the third sand wave in the train. In the original model, this ratio equals 1.33 whilst the sand wave in the modified model is more asymmetric, with the ratio being equal to 2.34.

From visual inspection of figure 3, we can say the first bump presents a rather small linear growth in both models whilst the sand waves in the train present an initial exponential growth followed by a linear one (approximately). van den Berg et al. (2012) computed the initial exponential growth rate of the sand waves by finding the slope that fits the curve $ln(A/A_0)$ against t. This was helpful to compare their results with the growth rates computed by Falqués and Calvete (2005) (with a linear stability analysis). It was shown that growth rates predicted by van den Berg et al. (2012) were bigger by a factor 4 than those predicted by the linear stability analysis. We have also plotted the logarithmic amplitude curves (figure 6) and they show that, in the modified model, the initial exponential growth tends to saturate after a while. The averaged growth rate in the original model is $1.49yr^{-1}$ whilst, in the modified model, the averaged growth rate is $1.09yr^{-1}$, in better agreement with Falqués and Calvete (2005). The migration velocity exhibits a linear behavior in both models (not shown). An interesting behavior is that the migration velocity increases with smaller wavelengths, which is in accordance with previous findings (van den Berg et al., 2012).

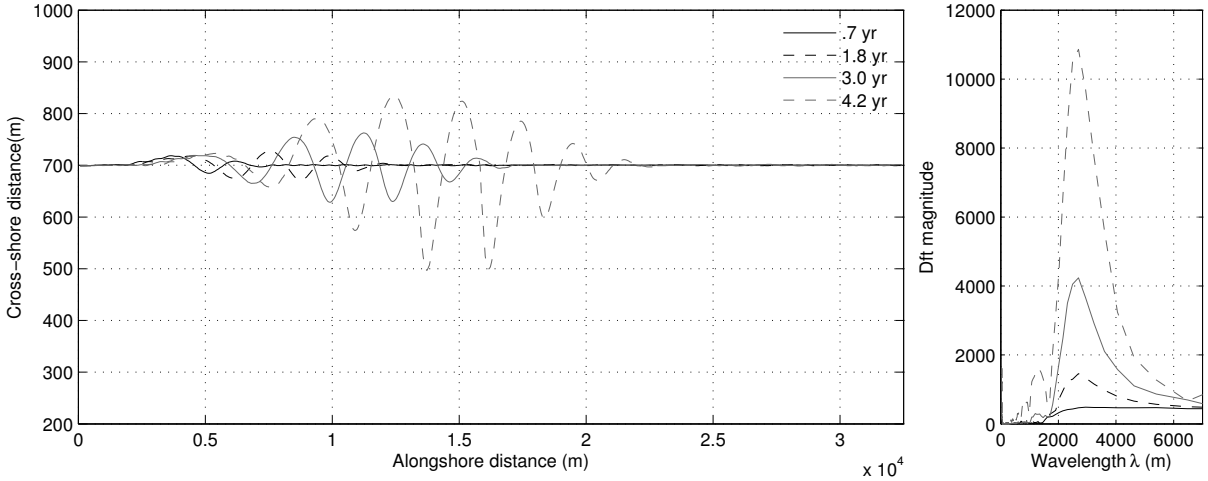

(a) original version

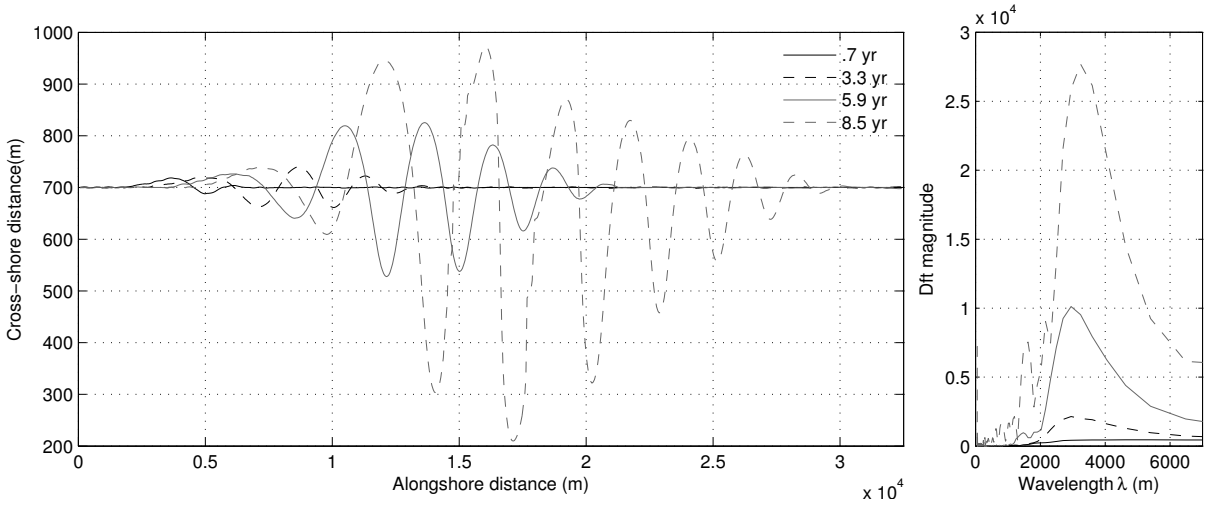

(b) modified version

Figure 4: Time evolution of the shoreline during the whole study period and the corresponding Fourier transformation for the two versions of the model.

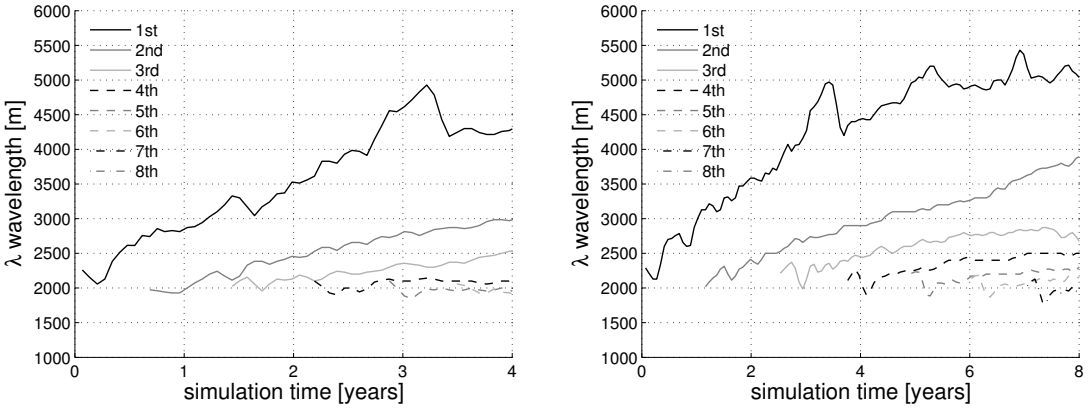

(a) original version **(b)** modified version

Figure 5: Time evolution of the wavelength of the individual sand waves of the sand wave train for the two versions of the model.

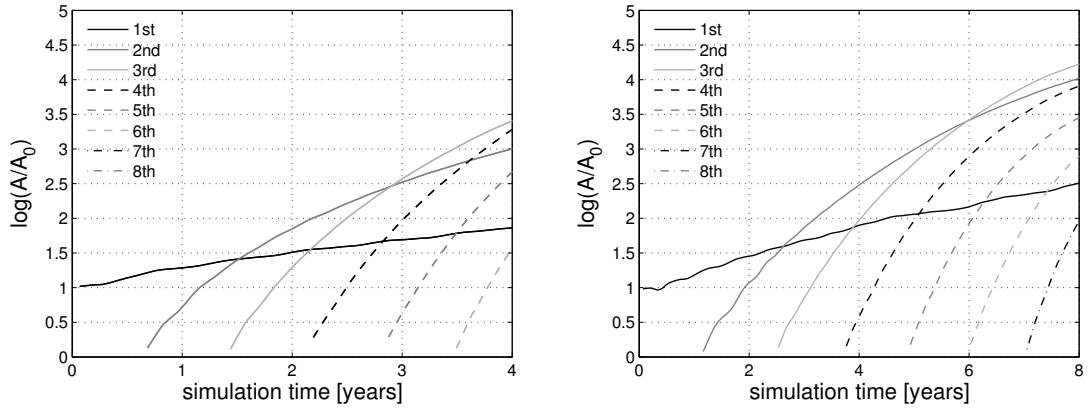

(a) original version **(b)** modified version

Figure 6: Time evolution of the $ln(A/A_0)$, where A_0 is the amplitude of the initial perturbation, of the individual sand waves of the sand wave train for the two versions of the model.

APPLICATION OF THE MODEL TO A STUDY SITE

Field site and data

The study site is located in the southeast of México, in Yucatán (Figure 7). The coast of this peninsula has several orientations and we focus on the northern coast of the peninsula, which is oriented west-east, with a small deviation of 12°. It presents a predominant direction of the alongshore transport from east to west.

Figure 7: Location of the study site. Images from Google Earth.

The wave climate is characterized by small waves of low periods, with an average of H_s = 0.6 m , T_p = 3.9 s and an incident angle respect to the shore normal θ = 42° (Figure 8). Wave conditions have been measured during the last two years at a buoy located at 8 m depth and the angles are originally measured with respect to the North and clockwise. Since the shoreline has an orientation of 78° grades with respect to the North, waves from 78°-258° do not reach the shore and they are not taken into account for the computation of the average wave direction.

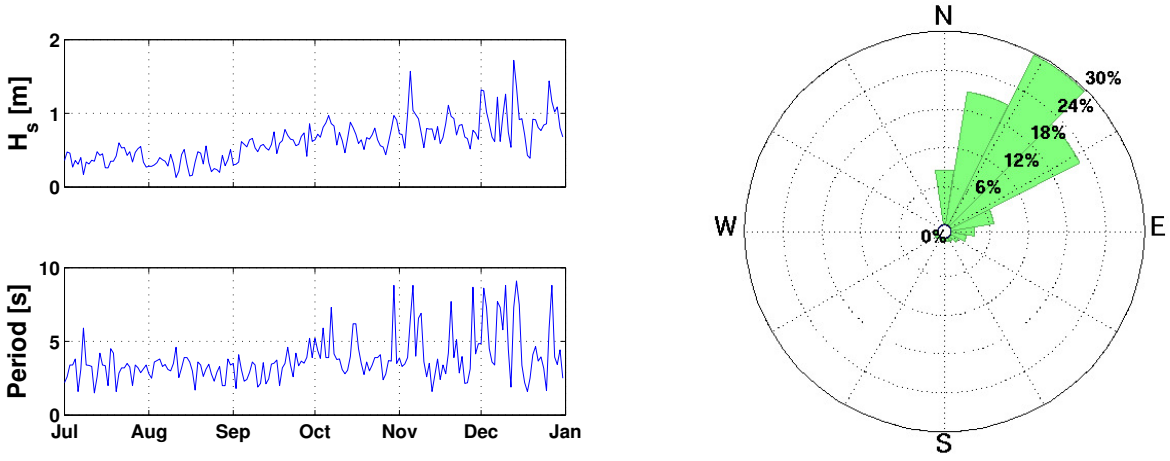

Figure 8: Wave data measured in a buoy located at 8 m depth in front of Chelém.

The sediment is characterized by a D_{50} = 0.2 mm outside the breaking zone. Under the site wave conditions, such sediment sizes can be moved at a maximum depth of 7 m, and we take this as the depth of closure D_c. From a measured bathymetry of Chelém we extract an average profile by previously rotating it 12°. The profile exhibits an orientation change at a depth of ~ 5 m (Figure 9).

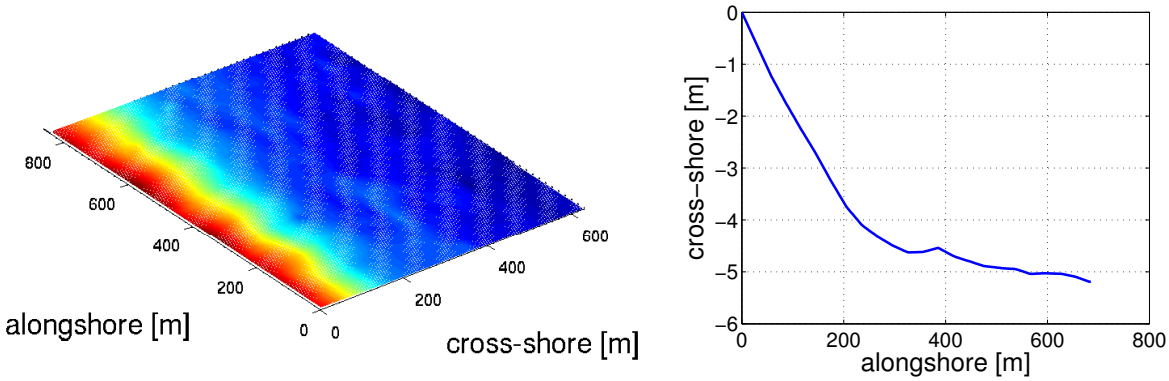

Figure 9: Bathymetry from Chelém (left) and its average profile (right).

Finally, we digitized shorelines along 15 km of the northern Yucatán coast from Google Earth. The shorelines available in this area correspond to the years 2004, 2010, 2011 and 2012 (Figure 10). We noticed that a rectification of this data was needed due to a deviation of the coordinates extracted from one year to the next. For this, we took the corners of a building as control points and we rectified all data sets with respect to these control points. The maximum difference between the same control point in different years was 15 m.

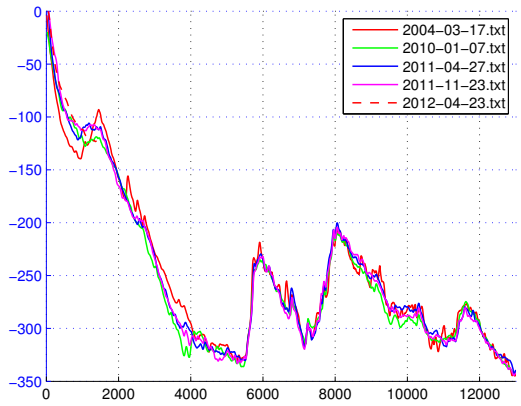

Figure 10: Shorelines digitized from Google Earth images of Chelém coast of five different dates. The x axis corresponds to the mean shoreline orientation of the stretch where the undulations are located.

The most clear signal of sand waves are three undulations in the area of Chelém. The two largest undulations have a similar shape, a wavelength of 2.2 km and an amplitude of 90 m (Figure 10 and 11)). A third smaller undulation can also be observed more to the east. The rest of the shorelines analyzed (up to 15 km) also show undulations at a km-scale but they are less clear. When analyzing the time evolution of the shorelines (with the available years 2004-2012), we do not observe a clear migration or growth.

Model results

In order to analyze the potential instability along this coast we use the same parameters as the default experiment in section 3 with the same initial perturbation but applying the averaged wave climate measured at the study site, H_s = 0.8 m, T_p = 4 s by mistake we took a slightly bigger H_s. This would only affect

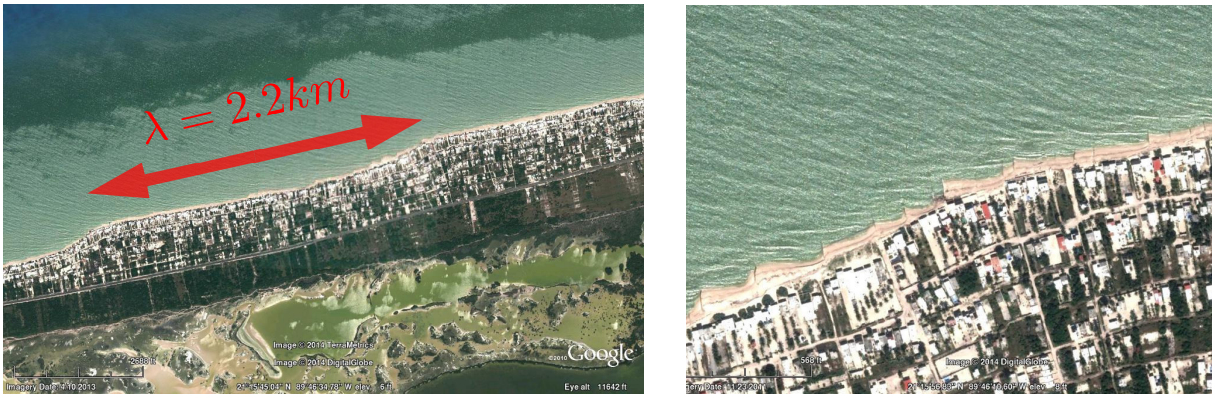

Figure 11: Google Earth image of the undulations in Chelém shoreline (left) and zoom of the undulation of the right to show the illegal groins (right).

the growth rate of the sand waves but not the transition from stable to unstable. For the wave incidence angle, θ_∞, we apply three different values: 42°, 47° and 52°. A modified Dean profile is adjusted to the average profile in Figure 8, with the shoreline slope being $\beta = 0.0167$ and a depth of 10 m being imposed at an offshore distance of 800 m. This Dean profile fits the observed profile up to 5 m depth. The modeled domain is of 780 m by 25000 m.

In the numerical experiment with a wave incidence angle of 42° the initial bump diffuses in 5 yr without generating a sand wave train. Thereby, the coast is stable under the averaged angle measured at the study site. For a wave incidence angle of 47° a wave train is generated with a wavelength of 3.5 km, an amplitude of only 6 m and a celerity of 0.29 km/yr. This small amplitude, which is maintained along 30 yr of simulation, suggests that the coast is in the limit of instability under this wave angle. For a wave incidence angle of 52°, a the sand wave train is clearly generated with a wavelength of 3.5 km, a growth rate of 0.8 m/yr and a celerity of 0.18 km/yr (Figure 12).

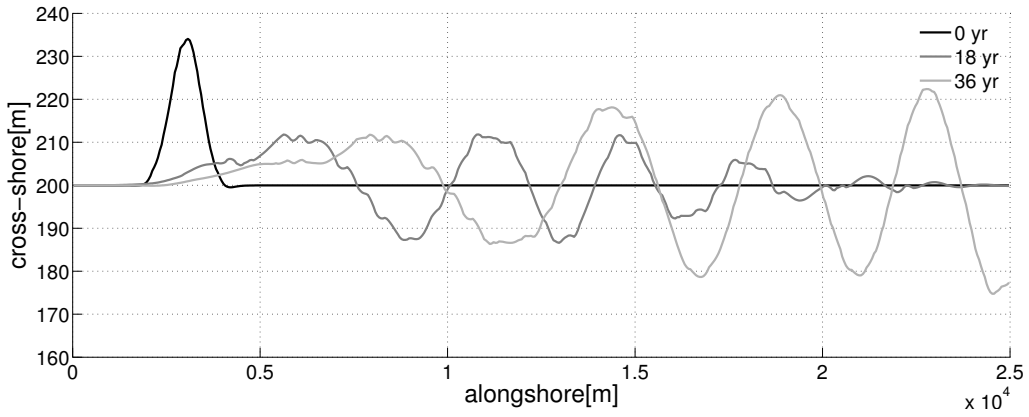

Figure 12: Time evolution of the shoreline obtained with the modified model when we apply it to the bathymetric and wave conditions measured in Chelém ($H_s = .8m$ $T_p = 4s$ $\theta = 52^o$).

Discussion

The shoreline at Chelém shows three sand waves and the rest of analyzed shorelines of the northern Yucatán coast also show small-amplitude undulations. In the available observations (from 2004 to 2012), the observed sand waves do not show growth or migration. We here discuss such behavior in view of the obtained model results. With the measured averaged wave climate, the model predicts diffusion of the initial perturbation. This suggests that HAWI would not trigger the formation of sand waves at the northern Yucatan coast. However, applying an incidence angle only 5^o larger than the observed one, the model

predicts the formation of a sand wave train with undulations of very small amplitude (6 m), which show no growth in 30 yr. With $\theta_\infty = 52^o$ (10^o larger than the observed value), the instability is clear, presenting a small but stable growth of 1.5 m/yr. Thereby, it could be that the shoreline at northern Yucatán coast is in the limit of instability or slightly unstable but that the short time period analyzed in the shoreline data does not allow to visualize the growth and migration. Note that in previous analysis of HAWI on natural coasts with clear shoreline sand waves, the different authors also had to exaggerate the conditions that favors instability: a greater depth of closure at Denmark, a lower wave period at the eastern African coast (Ribas et al., 2012) or a higher wave incidence angle (Kaergaard and Fredsoe, 2013). In the present study, instability occurs for wave incidence angles higher than the observed ones. Wave conditions might have been different in the past, when sand waves might be forming. Another phenomenon that could favor the observed static behavior of the sand waves in Chelém is related with human interventions. The local population constructed several illegal groins along the Yucatán coast (more than 100 in Chelém). Despite not having information about the construction dates of the illegal groins there is visual evidence of their existence in the Google Earth images (Figure 11). In fact, it is possible that the groins were initially constructed in order to prevent beach erosion linked to the troughs of alongshore migrating sand waves. The corresponding interruption of the alongshore transport, could have frozen the coast dynamics at Chelém. With the present information we can not discard nor confirm the presence of HAWI in this coast. Further analysis should me made. Firstly, historical information is necessary to discard the possibility that the undulations in Chelém are due to a geological constraint. Secondly, simulations representing more accurately the reality of the site should be performed. For example, the modified Dean profile used adjusts very well the average profile up to 5 m depth but farther offshore it greatly deviates, implying an effect on wave transformation. A profile that contains the abrupt change of orientation should be used. A synthetic wave climate is also necessary due to the great importance of energetic waves in this site ($> H_s = 1m$) whose effect is diminished by the average. Finally, the potential effect of the groins to slow or even freeze the sand wave dynamics could be studied with the model by modifying the shape function $f(x_c)$ in equation (5) to simulate the decrease of the alongshore transport.

CONCLUSIONS

An extension of the previous Q2D-morfo model of van den Berg et al. (2012), which can model the dynamics of km-scale shoreline sand waves, has been presented. The main changes are the introduction of a "fuzzy shoreline algorithm" and the modification of the direction of the cross-shore sediment transport, which now points in the local cross-shore direction. As a result, the model satisfactorily describes the dynamics of sand waves with larger amplitudes and larger asymmetry, compared to those described by van den Berg et al. (2012). The wavelengths are similar but the growth rates are smaller in the modified model, in better agreement with previous linear stability analysis (Falqués and Calvete, 2005). Besides, in the modified model some of the sand waves show a tendency to growth saturation. In order to compare the model results with observations, a 15 km stretch of the northern coast of Yucatán (México) has been studied. The shoreline in the area of Chelém have three sand waves of about 2.2 km in wavelength and about 100 m in amplitude (from crest to trough), which do not show appreciable migration or growth during the observation period (2004 to 2012). Undulations with similar characteristics are visible in the rest of the analyzed stretch. Model results obtained applying the modified model to the bathymetric and averaged wave conditions observed in Yucatán indicate shoreline stability. However, increasing slightly the incident wave angle caused the formation of small amplitude sand waves that persisted for a long time with a very small growth rate. This brings us to conclude that this coast might be at the threshold for instability, which imply that small changes in wave climate could either trigger or suppress the formation of sand waves. For example, sand waves created by a shoreline instability in the past could be now inactive. Finally, the construction of illegal groins to prevent erosion could also have frozen the dynamics of sand waves originated in the past.

ACKNOWLEDGMENTS

This research has been funded by the Spanish Ministerio de Ciencia e Innovación, through the research project CTM2012-35398. The first author is supported by a scholarship of the mexican government institution CONACYT. We thank Dr. Tonatiuh Mendoza for the wave data provided.

References

A. Ashton, A. B. Murray, and O. Arnault. Formation of coastline features by large-scale instabilities induced by high-angle waves. *Nature*, 414:296–300, 2001.

P. Bruun. Migrating sand waves or sand humps, with special reference to investigations carried out on the Danish North Sea Coast. In *Coastal Eng. 1954*, pages 269–295. Am. Soc. of Civ. Eng., 1954.

G. Coco and A. B. Murray. Patterns in the sand: From forcing templates to self-organization. *Geomorphology*, 91(271-290), 2007.

A. Falqués and D. Calvete. Large scale dynamics of sandy coastlines. Diffusivity and instability. *J. Geophys. Res.*, 110(C03007), 2005. doi:10.1029/2004JC002587.

D. Idier and A. Falqués. How kilometric sandy shoreline undulations correlate with wave and morphology characteristics: preliminary analysis on the atlantic coast of africa. *Advances in Geosciences*, 39:55–60, 2014. doi:10.5194/adgeo-39-55-2014.

K. Kaergaard and J. Fredsoe. Numerical modeling of shoreline undulations part 1: Constant wave climate. *Coastal Eng.*, 75:64–76, 2013.

K. Kaergaard, J. Fredsoe, and S. B. Knudsen. Coastline undulations on the West Coast of Denmark: Offshore extent, relation to breaker bars and transported sediment volume. *Coastal Eng.*, 60:109–122, 2012.

P. D. Komar. *Beach Processes and Sedimentation*. Prentice Hall, Englewood Cliffs, N.J., second edition, 1998.

R. Pelnard-Considère. Essai de theorie de l'evolution des formes de rivage en plages de sable et de galets. In *4th Journees de l'Hydraulique, Les Energies de la Mer, Paris*, volume III(1), pages 289–298. Société Hydrotechnique de France, 1956.

F. Ribas, H. E. de Swart, D. Calvete, and A. Falqués. Modeling and analyzing observed transverse sand bars in the surf zone. *J. Geophys. Res.*, 117(F02013), 2012. doi:10.1029/2011JF002158.

N. van den Berg, A. Falqués, and F. Ribas. Modelling large scale shoreline sand waves under oblique wave incidence. *J. Geophys. Res.*, 117(F03019), 2012. doi:10.1029/2011JF002177.